



HAL
open science

Passively Q-switched Er:YAG laser operating at 1617 nm at low pump power level

Adrien Aubourg, Julien Didierjean, Nicolas Aubry, François Balembois,
Patrick Georges

► **To cite this version:**

Adrien Aubourg, Julien Didierjean, Nicolas Aubry, François Balembois, Patrick Georges. Passively Q-switched Er:YAG laser operating at 1617 nm at low pump power level. *Journal of the Optical Society of America B*, 2014, 31 (12), pp.3131-3137. 10.1364/JOSAB.31.003131 . hal-01305579

HAL Id: hal-01305579

<https://hal-iogs.archives-ouvertes.fr/hal-01305579>

Submitted on 21 Apr 2016

HAL is a multi-disciplinary open access archive for the deposit and dissemination of scientific research documents, whether they are published or not. The documents may come from teaching and research institutions in France or abroad, or from public or private research centers.

L'archive ouverte pluridisciplinaire **HAL**, est destinée au dépôt et à la diffusion de documents scientifiques de niveau recherche, publiés ou non, émanant des établissements d'enseignement et de recherche français ou étrangers, des laboratoires publics ou privés.

Passively Q-switched Er:YAG laser operating at 1617 nm at low pump power level

Adrien Aubourg,^{1,2,*} Julien Didierjean,² Nicolas Aubry,² François Balembois,¹ and Patrick Georges¹

¹Laboratoire Charles Fabry, Institut d'Optique, CNRS, Univ Paris-Sud—2 Av A. Fresnel, F-91127 Palaiseau Cedex, France

²Fibercryst—Parc d'activité Wilson, Bât A1, 31 Rue Wilson, F-69150 Decines-Charpieu, France

*Corresponding author: adrien.aubourg@institutoptique.fr

We carried out an experimental study of an Er:YAG laser that is passively Q-switched by Cr:ZnSe saturable absorbers and pumped at 1470 nm by a 14 W laser diode. The 1617 nm emission is selected by an appropriate combination of transmissions of the saturable absorber and of the output coupler. With an accurate comparison between actively Q-switched and passively Q-switched operations and with Cr:ZnSe transmission measurements, we demonstrated by experiments and by simulations that the output energy is strongly dependent on the Cr:ZnSe temperature. With a better cooling of the Cr:ZnSe crystal heated by residual pump and signal absorption, the energy per pulse can be doubled, from 110 to 220 μJ , at a repetition rate of 800 Hz.

1. INTRODUCTION

The need for eye-safe laser sources operating in an atmospheric transmission window can be addressed by Er:YAG solid-state lasers emitting at 1.6 μm . Such lasers can be optically pumped by an Er:Yb fiber laser at 1533 nm [1], or by high power laser diodes at 1533 nm [2] or at 1470 nm [3]. Multimillijoule pulses have been successfully obtained in actively Q-switched (AQS) operation around 100 Hz, with large setups and overall electric consumption of several hundred watts.

However, some military applications, including lidar, telemetry or active imaging, require compactness and low electrical consumption. Hence, the use of a fiber laser or a high-power laser diode as a pump source is prohibited. Similarly, acousto-optic modulators (AOMs) or electro-optic modulators cannot be used to generate Q-switched giant pulses. In this context, a low power pump diode (~ 15 W) combined with a saturable absorber for passive Q-switching (PQS) is a good candidate for a compact laser emitter with an electrical consumption below 100 W.

Er:YAG crystal can emit at 1645 nm or at 1617 nm. The former is easier to generate since the inversion population ratio needed to reach the transparency is 9% instead of 15% at 1617 nm. However, at 1645 nm, the laser beam is slightly absorbed by methane [4], whereas 1617 nm is free of absorption in the atmosphere (Fig. 1). From the HITRAN database, the absorption coefficient of a laser beam whose spectrum is 0.3 nm large is around $5 \times 10^{-7} \text{ cm}^{-1}$ at 1645.2 nm and $1 \times 10^{-7} \text{ cm}^{-1}$ at 1617.0 nm. Hence, the range of a lidar system can be increased by a factor 5 only by controlling the wavelength at 1617 nm. It is a key for an eye-safe long-range laser emitter with low power consumption.

Among saturable absorbers operating around 1.6 μm , one can consider cobalt-doped crystals like Co:ZnSe, Co:ZnS [5], and Co:MgAl₂O₄ (Spinel) [6] or chromium-doped crystals

like Cr:ZnSe or Cr:ZnS, which have the benefit of a lower excited-state absorption cross section. Among the Cr²⁺ crystals, Cr:ZnSe is the most known, particularly for its wide emission band around 2.4 μm [7] allowing tunable mid-infrared cw oscillators [8,9], femtosecond oscillators, and amplifiers with hundreds of femtoseconds pulse duration [10–12]. Er:YAG PQS operation has already been successfully achieved with Cr:ZnSe crystals: a pulse energy of 235 μJ has been generated under a pump optical power of 16 W from a fiber laser [13], and 500 μJ under 40 W of laser diode optical power [14]. To the best of our knowledge, the 1617 nm laser emission has not been demonstrated yet with a low power (< 15 W) laser diode.

In this paper, we propose a study of low-power (14 W) diode-pumped Er:YAG laser passively Q-switched with a Cr:ZnSe at 1617 nm. First, we present a comparative study between AQS and PQS based on experimental results (Section 2) and simulations (Sections 3 and 4). Next (Section 5), we study the transmission of the Cr:ZnSe versus the temperature. We conclude finally on the performance of the PQS Er:YAG laser versus Cr:ZnSe temperature explaining the strong difference of output performances between PQS and AQS operations (Section 6).

2. LASER SOURCE PERFORMANCE

Our Er:YAG laser (Fig. 2) is pumped by a laser diode emitting 14 W at 1470 nm, coupled into a 100 μm core diameter fiber with a numerical aperture of 0.22. To our knowledge, it is one of the lowest laser diode powers ever used to pump an Er:YAG laser. The pump beam is focused a few millimeters inside the crystal with two doublets of 50 and 100 mm of focal length, leading to a pump spot diameter of 200 μm . The 0.5 at. % erbium-doped YAG crystal is 30 mm long with a diameter of 750 μm . It is embedded inside a water-cooled copper plate (TARANIS module from Fibercryst). The M1 mirror is a

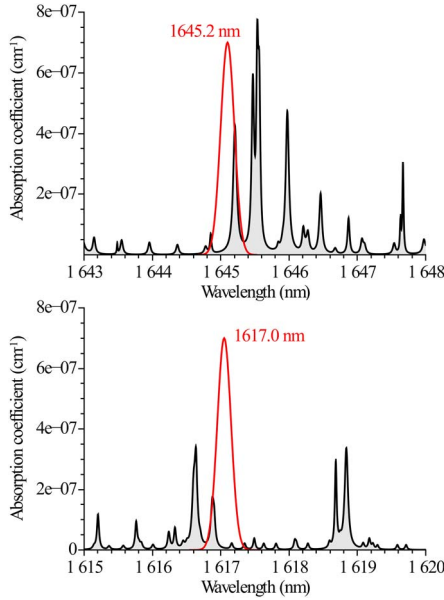


Fig. 1. Absorption coefficient of the atmosphere (black) extracted from the HiTRAN database versus the wavelength around 1645 nm (top) and 1617 nm (bottom). An Er:YAG laser beam spectrum with an arbitrary spectral width of 0.3 nm is superimposed (red) at 1645.2 nm and 1617.0 nm.

dichroic meniscus with a radius of curvature of 50 mm. It has a high reflectivity for the laser wavelength over the 1600–1650 nm range and a high transmission for the pump wavelength over the 1440–1500 nm range. The output coupler M2 has a radius of curvature of 100 mm and a reflectivity of 80% for both 1645 and 1617 nm wavelengths. The distance between M1 and M2 is 140 mm.

At full pump power, the thermal focal length in Er:YAG has been evaluated to be $400 \text{ mm} \pm 50 \text{ mm}$ approximately. This large value can be explained by the low pump power level combined with the good heat extraction of the TARANIS module. Consequently, the thermal lens does not affect significantly the beam waist in the Er:YAG (calculated diameter of $210 \mu\text{m}$).

We first investigated the AQS regime. For this purpose, we used a 60 mm long quartz AOM. We inserted a $100 \mu\text{m}$ thin etalon to select the emission wavelength (1617 or 1645 nm).

Figure 3 shows the performance of the AQS Er:YAG laser for different repetition rates. At 1645 nm, despite the low pump power level, the energy reaches $900 \mu\text{J}$ with a repetition rate of 100 Hz and a pulse duration of 32 ns (28 kW peak power). These results are fairly good compared to the state

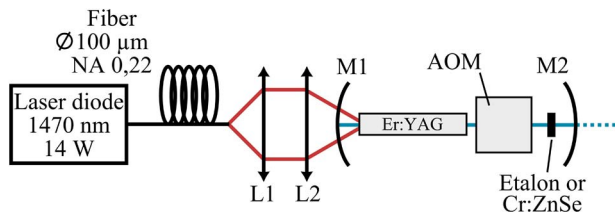


Fig. 2. Schematic setup of the Er:YAG source. An etalon is used in case of AQS regime to force the 1617 nm emission. The cavity can be passively *Q*-switched with a Cr:ZnSe saturable absorber. In this case, it is inserted in place of the etalon and the AOM is kept inactive inside the cavity for direct comparison purpose.

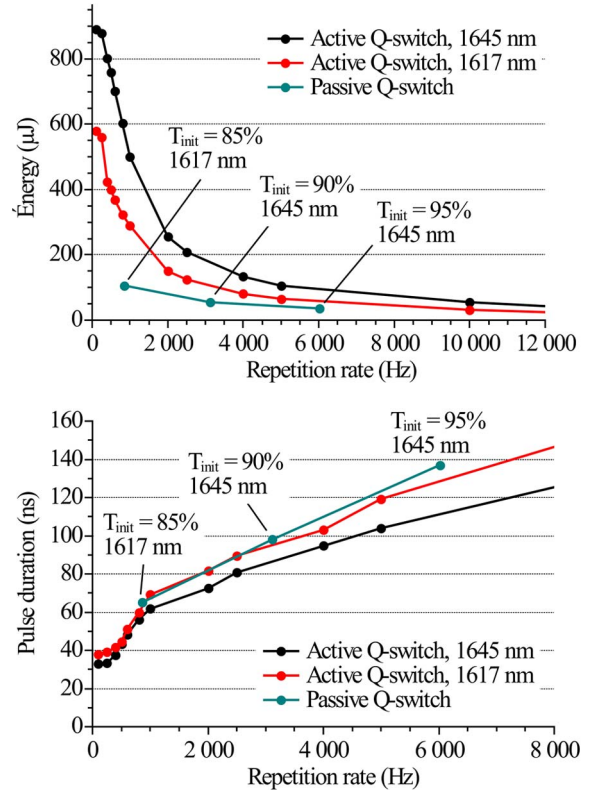


Fig. 3. Output energy (top) and pulse duration (bottom) of the Er:YAG laser at 1645 nm (black) and 1617 nm (red) for AQS and PQS (blue) operations versus the repetition rate. Saturable absorber small signal transmissions are 95%, 90%, and 85%. A wavelength shift occurs for 85% small signal transmission.

of the art, but no direct comparison could be done as no Er:YAG cavity has been reported with such low diode-pump power. At 1617 nm with the same repetition rate, the output energy is $550 \mu\text{J}$ and the pulse duration is 36 ns (15 kW peak power). The decrease in energy is mainly caused by the higher threshold at 1617 nm compared to 1645 nm (Fig. 4). At both wavelengths, the measured beam quality factor M^2 is 1.6.

In order to compare AQS and PQS under the same conditions, the AOM is kept inactive inside the cavity. Cr:ZnSe crystals with doping concentration of $15 \times 10^{18} \text{ cm}^{-3}$ and small signal transmissions of 95%, 90%, and 85% are consecutively inserted in the cavity in place of the etalon. Their size is around $3 \text{ mm} \times 3 \text{ mm} \times 0.8 \text{ mm}$.

The emission wavelength is freely chosen by the cavity, depending on the gain and the inserted losses. Laser emission occurs at 1645 nm for saturable absorbers with small signal transmission of 95% and 90%. This emission wavelength is shifted to 1617 nm when using the saturable absorber whose small signal transmission is 85%. This effect has already been observed previously [13,14], and has two origins. First, the slope of the Cr:ZnSe absorption cross section is raising between 1617 and 1645 nm [7]. We considered absorption cross sections at 1645 and 1617 nm to be $0.95 \times 10^{-22} \text{ m}^2$ and $0.8 \times 10^{-22} \text{ m}^2$, respectively, [15]. Hence, the Cr:ZnSe saturable absorber favors the emission at 1617 nm as its small signal transmission at 1645 nm is higher. Second, the insertion of a saturable absorber having a low small signal transmission (85%) increases the intracavity losses and consequently increases the gain needed to reach the threshold, favoring

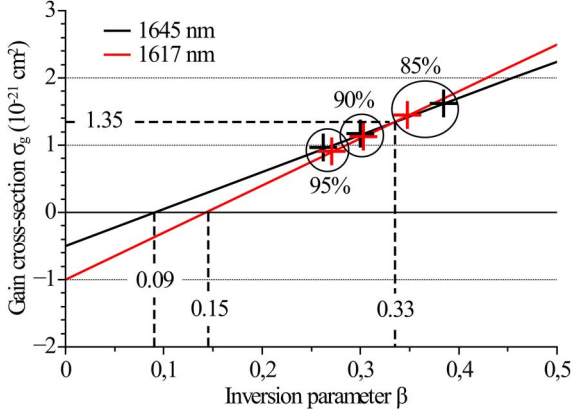


Fig. 4. Gain cross sections of Er:YAG at 1645 and 1617 nm versus the inversion parameter β , which represents the erbium ions at the excited state over the total number of ions. Values of cross sections extracted from [16]. Crosses indicate the gain cross section at threshold for the different configuration.

the laser transition with the highest emission cross section (1617 nm). To illustrate the wavelength shifting from these two causes, we plotted the gain cross section versus the inversion parameter β at 1645 and 1617 nm (Fig. 4):

$$\sigma_g(\lambda) = \beta \cdot \sigma_e(\lambda) - (1 - \beta) \cdot \sigma_a(\lambda). \quad (1)$$

By assuming a homogeneous population inversion in the gain medium for a better understanding, we can write the threshold gain cross section needed to start the laser oscillation inside the cavity:

$$\sigma_g^{\text{th}} = \frac{-\ln(R \cdot L \cdot T_{\text{sa}}^2)}{2 \cdot n_t \cdot l}, \quad (2)$$

with R being the output reflection rate, L the passive losses, l the length of the Er:YAG crystal, and n_t the doping density. T_{sa} is the small signal transmission of the saturable absorber. The numerical applications for each saturable absorber, and for both emission wavelengths, are shown in Fig. 4. The lasing wavelength is determined by the gain cross section at threshold with the smallest inversion parameter β . In the case of Q-switch regimes with the 95% and 90% small signal transmission saturable absorbers, the emitted wavelength is 1645 nm. For the darker saturable absorber, it is 1617 nm.

Consequently, the wavelength selection can be done without any additional wavelength selector, increasing the efficiency and the simplicity of the source.

The energy is measured for the three saturable absorbers at full pump power. The three sets of experimental data are given in Fig. 3. Compared to AQS, the pulse duration is the same versus the repetition rate. However, the energy is dramatically lowered.

3. DESCRIPTION OF THE NUMERICAL MODELIZATION

To go further with this investigation and explain this energy drop, we carried out simulations of the pulse energy versus the repetition rate. The numerical model for AQS four-levels systems depicted in [17] has been modified for the erbium quasi-three-levels architecture with upconversion [18,19],

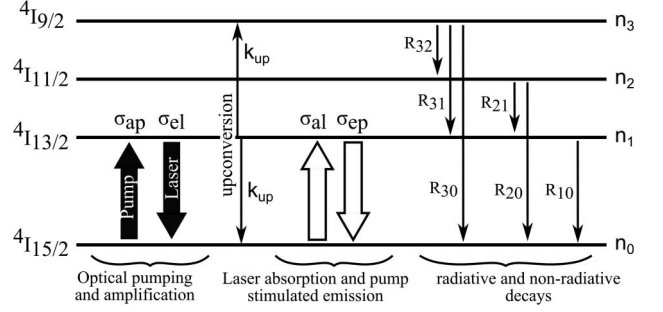


Fig. 5. Energy levels of the Er:YAG crystal for the numerical simulation.

laser reabsorption, and pump stimulated emission. Figure 5 gives the considered energy levels and rates. Equation (3) gives the corresponding rate equations:

$$\begin{aligned} \frac{dn_3}{dt} &= -(R_{32} + R_{31} + R_{30})n_3 + k_{\text{up}}n_1^2, \\ \frac{dn_2}{dt} &= R_{32}n_3 - (R_{21} + R_{20})n_2, \\ \frac{dn_1}{dt} &= R_{31}n_3 + R_{21}n_2 - R_{10}n_1 - 2k_{\text{up}}n_1^2 + (\sigma_{\text{ap}}n_0 - \sigma_{\text{ep}}n_1)I_p \\ &\quad + (\sigma_{\text{al}}n_0 - \sigma_{\text{el}}n_1)I_l, \\ \frac{dn_0}{dt} &= -\sum_{i=1,2,3} \frac{dn_i}{dt}. \end{aligned} \quad (3)$$

The equation system is solved for each subvolume $V(\mathbf{r})$ of the crystal. In our specific case which takes benefits of the cylindrical geometry of the gain media and the fiber coupled pumping to lighten the computations, $V(\mathbf{r})$ could be written $2\pi \cdot r \cdot \Delta r \cdot \Delta z$ (Fig. 6). The values n_i , I_p , I_l , and σ_{**} are dependent of the spatial variable \mathbf{r} . The Er:YAG cross-sections values σ_{**} are extracted from [16]. The pump intensity I_p inside the whole crystal is obtained from a homemade ray tracing software. The laser intensity I_l is calculated from the number of photons inside the cavity Φ , the effective mode volume V_{eff} , and the normalized field shape (obtained through the Gaussian mode analysis) $u(\mathbf{r})$ [17]. I_l is given by the following equation:

$$I_l(r, z, t) = \frac{\Phi(t)n_{\text{Er:YAG}}hc^2}{V_{\text{eff}}\lambda} |u(r, z)|. \quad (4)$$

The quantity Φ evolves according to the population inversions of the crystal and the lifetime of the photon inside the cavity τ_c :

$$\frac{d\Phi}{dt} = \sum_r (\sigma_{\text{el}}n_1 - \sigma_{\text{al}}n_0)I_l V(r) - \frac{\Phi}{\tau_c}. \quad (5)$$

τ_c is calculated from the photon round-trip time τ_r , the logarithmic passive losses L , and the output reflection rate $R = -\log(r_c)$:

$$\tau_c = \frac{\tau_r}{L + R}. \quad (6)$$

Equations (3)–(6) can lead to the time-resolved instantaneous power of the laser source, from its start to its steady-state

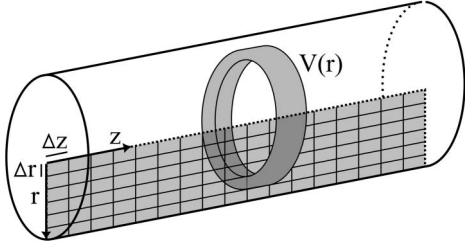


Fig. 6. Numerical modeling of the Er:YAG crystal. All the physical quantities are reduced to 2D tabulars to lighten the computations.

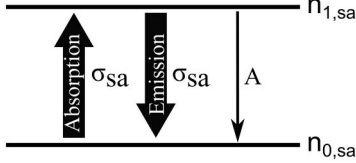


Fig. 7. Energy levels of the Cr:ZnSe crystal for the numerical simulation.

regime. To simulate the Q-switched operation, additional logarithmic losses in the cavity must be added. They can be time-dependent (for AQS) or laser intensity-dependent (for PQS). To simulate the latter, we introduce a set of two equations that describe the physical behavior of the Cr:ZnSe saturable absorber, assumed to be a simple two-level system (Fig. 7):

$$\begin{aligned} \frac{dn_{1,sa}}{dt} &= n_{0,sa}\sigma_{sa}I_l - n_{1,sa}\sigma_{sa}I_l - An_{1,sa}, \\ \frac{dn_{0,sa}}{dt} &= -\frac{dn_{1,sa}}{dt}. \end{aligned} \quad (7)$$

As our Cr:ZnSe samples are relatively highly concentrated ($15 \times 10^{18} \text{ cm}^{-3}$), concentration quenching occurs for excited Cr^{2+} ions: from [7], we estimated the upper-state lifetime at $4 \mu\text{s}$ (instead of commonly reported $5.5 \mu\text{s}$). We neglected the excited-state absorption that may occur in Cr:ZnSe as it is very low compared to ground-state absorption [20]. In addition, unlike the Er:YAG, these equations are not spatially resolved. Hence, spatial filter effect, which may come from low laser intensity on the edge of the beam, is also neglected by the simulation.

Finally, from the Cr:ZnSe population inversion, one can calculate the logarithmic losses L_{sa} it introduces in the cavity knowing its length l_{sa} :

$$L_{sa} = -2(n_{1,sa} - n_{0,sa})\sigma_{sa}l_{sa}. \quad (8)$$

4. COMPARISON OF EXPERIMENTAL RESULTS OF THE NUMERICAL MODELING

Figure 8 shows that AQS simulations fit well the experimental results by only providing a small adjustment on the laser beam waist diameter from 210 to 230 μm .

With the same fitting parameters as for AQS, simulations in PQS operation give lower energies, as expected by the PQS process itself. However, the simulated energy remains approximately two times higher than the experimental energy whatever the Cr:ZnSe crystal used (Fig. 9).

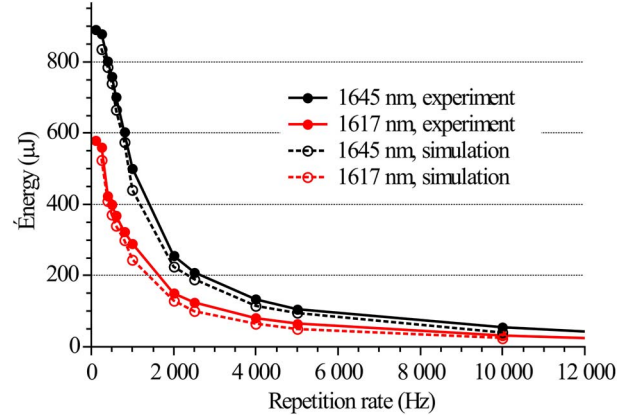


Fig. 8. Experimental (plain) and simulated (dashed) energy in AQS operation at 1645 nm (black) and 1617 nm (red).

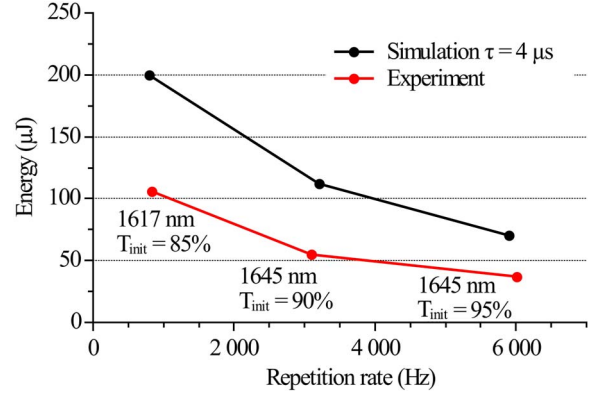


Fig. 9. Experimental and simulated PQS energies.

5. ORIGIN AND EXPERIMENTAL MEASUREMENT OF Cr:ZnSe TRANSMISSIONS VARIATIONS WITH TEMPERATURE

Our simulation indicates that another limiting process should be at stake. For this reason, we decided to measure the temperature of the Cr:ZnSe crystal during laser operation with an infrared camera. To our surprise, the temperature was around 150°C (Fig. 10). In fact, no attention was paid to the Cr:ZnSe heat dissipation, as it was simply mounted on an aluminum

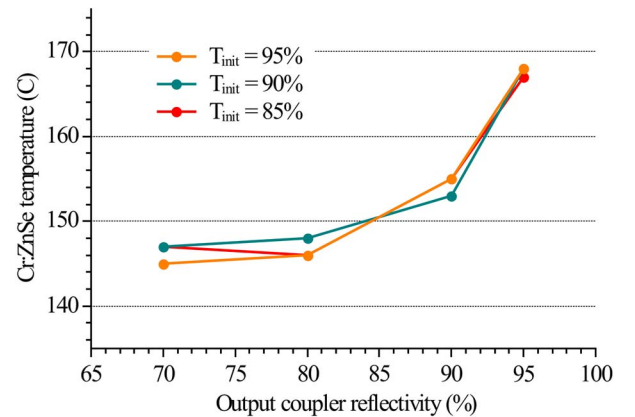


Fig. 10. Cr:ZnSe temperature in PQS operation versus the output coupler reflectivity, for different small signal transmission.

plate without cooling. This high temperature can be attributed to residual pump absorption (2 W are not absorbed by the Er:YAG crystal and are incident on the Cr:ZnSe and its mount). Moreover, Fig. 10 shows that the temperature varied with the output coupler. This indicates that absorption at the signal wavelength contributes also to the temperature increase: the higher is the output coupler reflectivity, higher is the intracavity signal and consequently higher is the absorption.

To go further with this study, we designed an experiment to measure the unsaturated and the saturated transmissions of the Cr:ZnSe crystal versus its temperature (Fig. 11). The study is concentrated on the “Tinit = 85%” Cr:ZnSe as it gives the highest energy at the desired wavelength (1617 nm). This time, the sample is mounted on a thermally controlled system including a thermoelectric cold plate (for cooling) and an oven (for heating over 200°C). The temperature of the Cr:ZnSe was measured by an infrared camera. It varied from 5°C to 220°C.

The transmission is probed by 250 ns, 8 kHz repetition rate, 20 μ J pulses at 1617 nm coming from the AQS laser developed previously. With a diameter of 1.4 mm (corresponding to a peak power density of 5.2 kW/cm²) we measured the unsaturated transmission, the saturation intensity being of the order of 15 kW/cm². To vary the incident peak power density, we modified the probe beam diameter with different lenses. We used a lens L3 with a 4 cm focal length (140 μ m diameter spot, 500 kW/cm² peak power density) to measure the saturated transmission. We also studied an intermediate configuration (400 μ m diameter spot, 65 kW/cm² peak power density) with a lens L3 of 10 cm focal length. Figure 12 shows the measured transmissions at 1617 nm versus the Cr:ZnSe crystal temperature.

For all temperatures, the unsaturated transmission is in good agreement with the Cr:ZnSe specifications: an unsatu-

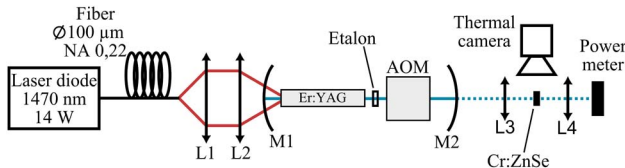


Fig. 11. Experimental setup for the unsaturated (without L3/L4 lenses) and saturated (with L3/L4 lenses) transmission measurements.

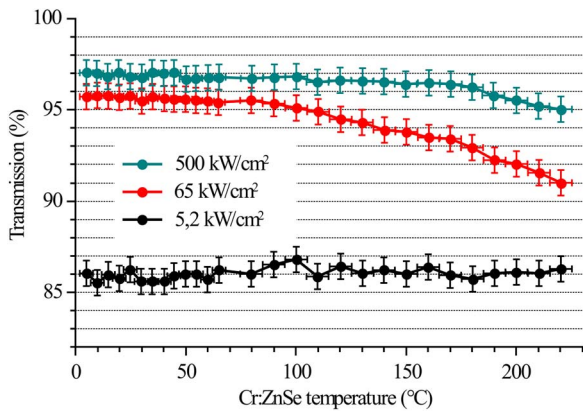


Fig. 12. Transmissions of a Cr:ZnSe (small signal transmission of 85%) in saturated and unsaturated regime at 1617 nm versus the temperature.

rated transmission close to 85% is observed. Between 5°C and 60°C, the saturated transmissions remain constant, the transmission at 500 kW/cm² being slightly higher. Above 60°C, the saturated transmissions decrease with the temperature. This indicates that the incident intensity is closer and closer to the saturation intensity.

The origin of the transmission decrease may lie in the upper-state lifetime reduction with the crystal temperature. Previous measurements showed that the lifetime decreases from 5.5 μ s to less than 1 μ s in the range 25°C–150°C because of thermal quenching [20]. As shown by Eq. (9), the saturation intensity I_{sat} of the saturable absorber is inversely proportional to the lifetime (h is the Planck constant, ν is the optical frequency of the signal, τ is the upper-state lifetime of the chromium ions, and σ_{sa} is the absorption cross section):

$$I_{\text{sat}} = h\nu/\tau\sigma_{\text{sa}}. \quad (9)$$

So thermal quenching corresponds to an increase of the saturation intensity by a factor of 5 between 25°C and 150°C, overcoming the value of the incident intensity (65 kW/cm²) at 150°C.

From relations (8) and (9), and from the measured transmissions (Fig. 12), we are able to fit the transmission curves with the upper-state lifetime as a parameter. We carried out the calculation for temperatures over 120°C, where the transmission decrease is significant compared to the transmission at room temperature. The estimated lifetime is reported in Fig. 13 for temperatures ranging from 120°C to 220°C. Those results are in accordance with the previous results from [20] and show a constant decrease for higher temperatures.

Thus the Cr:ZnSe lifetime decrease versus temperature may explain the low performance of the PQS laser. We carried out simulations of the output energy with a Cr:ZnSe lifetime of 200 ns instead of 4 μ s. Figure 14 shows that the simulations are very close to the experimental energies for the three different saturable absorbers and for the two emitted wavelengths (1617 and 1645 nm). This study highlights that the high temperature of the Cr:ZnSe strongly reduces the output energy in PQS operation. Therefore, cooling the Cr:ZnSe may increase the performance significantly. This is carried out in the next experiment.

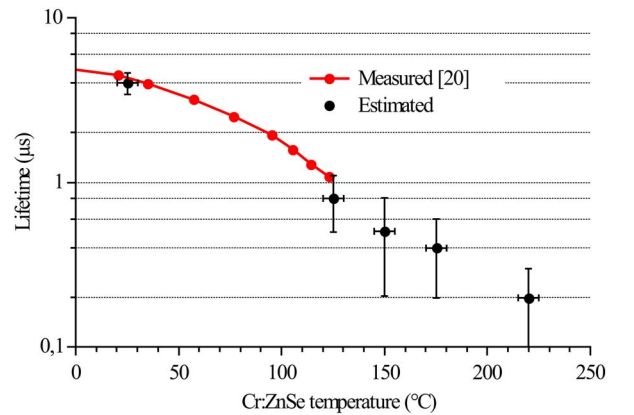


Fig. 13. Measured lifetime from [20] and estimated lifetime from our transmissions measurements of the Cr:ZnSe crystal versus its temperature.

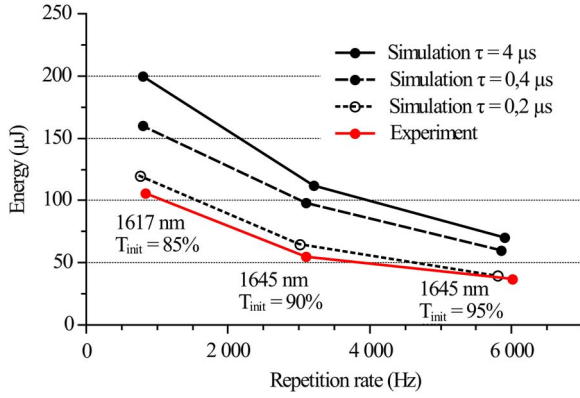


Fig. 14. Experimental and simulated PQS output energies for different Cr:ZnSe upper-state lifetime.

6. PASSIVELY Q-SWITCHED OSCILLATOR PERFORMANCES VERSUS Cr:ZnSe TEMPERATURE

We removed the AOM from our first setup (Fig. 2) and we reduced the cavity length down to 70 mm. The “ $T = 85\%$ ” Cr:ZnSe crystal temperature was controlled by a thermoelectric cold plate and an oven, and monitored thanks to a thermal camera. Figure 15 shows the pulse energy and the repetition rate for a temperature ranging from 5°C to 220°C . The repetition rate remains constant. It can be explained by the unsaturated transmission behavior being roughly independent of the temperature (Fig. 12). We observed that the energy strongly decreases while the temperature increases, as expected. Energy of $100\ \mu\text{J}$ is obtained for a temperature of 170°C , in agreement with the previous transmission measurements related to Fig. 12. The output energy is doubled by cooling the Cr:ZnSe at room temperature: this optimized output corresponds to an energy of $220\ \mu\text{J}$, a pulse duration of 32 ns, and a repetition rate of 800 Hz.

Figure 15 also presents the energy calculated from our simulation including the estimated lifetime for different temperatures coming from Fig. 13. The simulations show the right tendency with a significant discrepancy at high temperatures. This may come from uncertainty in the lifetime estimation and from other effects, like excited-state absorption.

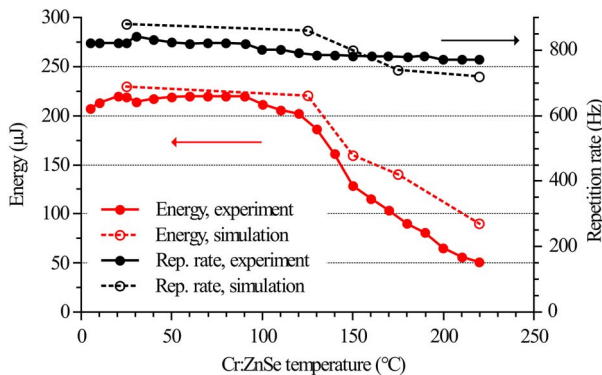


Fig. 15. Pulse energy (red) and repetition rate (black) of the PQS Er:YAG cavity versus the “ $T = 85\%$ ” Cr:ZnSe temperature. Output energies and repetition rates from simulations (dashed) for different estimated Cr:ZnSe lifetimes (Fig. 13) are also plotted.

7. CONCLUSION

In our quest to design an eye-safe and long-range laser emitter for Lidar applications, we reported a passively Q-switched Er:YAG laser diode-pumped at one of the lowest levels ever reported (only 14 W). Despite this pump power, we succeeded in PQS laser operation at 1617 nm without any additional wavelength selector in the cavity, by an appropriate choice of the transmissions of the output coupler and the saturable absorber. This specific wavelength emission enhances the atmospheric transmission range of the emitter by a factor of 5. Moreover, with an in-depth analysis including comparison between AQS and PQS experimental performance, and Cr:ZnSe saturable absorber transmissions measurements, we demonstrated that the PQS output energy is strongly dependent on the Cr:ZnSe temperature. The residual absorption at the pump wavelength and at the laser wavelength may cause a temperature increase of the Cr:ZnSe, reducing the upper-state lifetime and consequently strongly increasing the saturation intensity. At high temperature, the Cr:ZnSe is not completely bleached by the laser pulse, leading to additional losses and to an important energy decrease. By controlling the Cr:ZnSe temperature below 100°C , we were able to double the output energy: from $110\ \mu\text{J}$ without temperature control to $220\ \mu\text{J}$.

This work could lead to compact and efficient eye-safe emitters for applications requiring long-range transmission in the atmosphere. Specifically, microlaser architecture is a good candidate for such a laser source. Indeed, we showed that the cooling of the saturable absorber is a key to optimize the laser output performances, and this architecture usually cools the gain medium and the saturable absorber together. Additionally, the expected short pulse duration would give a better spatial resolution, and the short highly doped Er:YAG crystal could allow the use of direct nonfiber coupled laser diodes as a pump source.

ACKNOWLEDGMENTS

This work has been funded by the Direction Générale de l’Armement (112906173).

REFERENCES

1. J. W. Kim, D. Y. Shen, J. K. Sahu, and W. A. Clarkson, “Fiber-laser-pumped Er:YAG lasers,” *IEEE J. Sel. Top. Quantum Electron.* **15**, 361–371 (2009).
2. M. Eichhorn, “High-power resonantly diode-pumped CW Er³⁺:YAG laser,” *Appl. Phys. B* **93**, 773–778 (2008).
3. Y. Zheng, C. Gao, R. Wang, M. Gao, and Q. Ye, “Single frequency 1645 nm Er:YAG nonplanar ring oscillator resonantly pumped by a 1470 nm laser diode,” *Opt. Lett.* **38**, 784–786 (2013).
4. K. O. White and S. A. Schlausener, “Coincidence of Er:YAG laser emission with methane absorption at 1645.1 nm,” *Appl. Phys. Lett.* **21**, 419–420 (1972).
5. T. Y. Tsai and M. Birnbaum, “Co²⁺:ZnS and Co²⁺:ZnSe saturable absorber Q switches,” *J. Appl. Phys.* **87**, 25–29 (2000).
6. M. Němec, H. Jelinkova, J. Sulc, K. Nejezchleb, and V. Skoda, “Passive Q-switching at 1645 nm of Er:YAG laser with Co:MALO saturable absorber,” in *Proceedings of the International Quantum Electronics Conference and Conference on Lasers and Electro-Optics Pacific Rim* (2011), paper C552.
7. V. E. Kisel, V. G. Shcherbitsky, N. V. Kuleshov, V. I. Konstantinov, V. I. Levchenko, E. Sorokin, and I. Sorokina, “Spectral kinetic properties and lasing characteristics of diode-pumped Cr²⁺:ZnSe single crystals,” *Opt. Spectrosc.* **99**, 663–667 (2005).

8. Y. F. Dai, Y. Y. Li, X. Zou, Y. J. Dong, and Y. X. Leng, "High-efficiency broadly tunable Cr:ZnSe single crystal laser pumped by Tm:YLF laser," *Laser Phys. Lett.* **10**, 105816 (2013).
9. R. H. Page, K. I. Schaffers, L. D. DeLoach, G. D. Wilke, F. D. Patel, J. B. Tassano, Jr., S. A. Payne, W. F. Krupke, K.-T. Chen, and A. Burger, "Cr²⁺-doped zinc chalcogenides as efficient, widely tunable mid-infrared lasers," *IEEE J. Quantum Electron.* **33**, 609–619 (1997).
10. P. Moulton and E. Slobodchikov, "1-GW-peak-power, Cr:ZnSe laser," in *Conference on Lasers and Electro-Optics* (2011), paper PDP10.
11. N. Tolstik, E. Sorokin, and I. T. Sorokina, "Kerr-lens mode-locked Cr:ZnS laser," *Opt. Lett.* **38**, 299–301 (2013).
12. M. N. Cizmeciyan, J. W. Kim, S. Bae, B. H. Hong, F. Rotermund, and A. Sennaroglu, "Graphene mode-locked femtosecond Cr:ZnSe laser at 2500 nm," *Opt. Lett.* **38**, 341–343 (2013).
13. R. D. Stultz, V. Leyva, and K. Spariosu, "Short pulse, high-repetition rate, passively Q-switched Er:yttrium-aluminum-garnet laser at 1.6 microns," *Appl. Phys. Lett.* **87**, 241118 (2005).
14. A. Aubourg, J. Didierjean, N. Aubry, F. Balembois, and P. Georges, "Passively Q-switched diode-pumped Er:YAG solid-state laser," *Opt. Lett.* **38**, 938–940 (2013).
15. H. Cankaya, U. Demirbas, A. Erdamar, and A. Sennaroglu, "Absorption saturation analysis of Cr²⁺:ZnSe and Fe²⁺:ZnSe," *J. Opt. Soc. Am. B* **25**, 794–800 (2008).
16. M. Eichhorn, S. T. Fredrich-Thornton, E. Heumann, and G. Huber, "Spectroscopic properties of Er³⁺:YAG at 300–550 K and their effects on the 1.6 μm laser transitions," *Appl. Phys. B* **91**, 249–256 (2008).
17. M. Wohlmuth, C. Pflaum, K. Altmann, M. Paster, and C. Hahn, "Dynamic multimode analysis of Q-switched solid state laser cavities," *Opt. Express* **17**, 17303–17316 (2009).
18. S. Georgescu, O. Toma, and I. Ivanov, "Upconversion from the ⁴I_{13/2} and ⁴I_{11/2} levels in Er:YAG," *J. Lumin.* **114**, 43–52 (2005).
19. J. White and C. Mungan, "Measurement of upconversion in Er:YAG via z-scan," *J. Opt. Soc. Am. B* **28**, 2358–2361 (2011).
20. I. Sorokina, "Broadband mid-infrared solid-state lasers," in *Mid-Infrared Coherent Sources and Applications* (Springer, 2008), pp. 225–260.